

# Kinetics and Mechanism of Hydrogen Reduction of Lead-Silicate Slag



A. RUKINI, M.A. RHAMDHANI, G.A. BROOKS, A. VAN DEN BULCK,  
and T. VAN ROMPAEY

A systematic study on the microstructure evolution and kinetics analysis of PbO–SiO<sub>2</sub> slag reduction using hydrogen was conducted. The reduction was carried out on PbO–SiO<sub>2</sub> pellets (70 wt pct PbO–30 wt pct SiO<sub>2</sub>; or 38.6 mol pct PbO and 61.4 mol pct SiO<sub>2</sub>) using 15 pctH<sub>2</sub>/85 pctN<sub>2</sub> gas, with a flowrate of 500mL/min for various reaction time (30 minutes to 3 hours) isothermally at 300 °C to 700 °C. The kinetics and reaction mechanism were assessed by measuring the weight loss over reaction time and applying kinetics models on the data; supported by detailed samples characterizations. The results from microstructure observation show a viscous and blackish glass structure formed on the pellets when the reduction was carried out above softening point (glass transition temperature). This viscous structure appeared to reduce the overall reduction rate. The kinetics analysis shows that the reduction appeared to be a diffusion-controlled process. The activation energy,  $E_a$ , was calculated to be 70.7 kJ/mol at temperature range of 300 °C to 500 °C; while between 500 °C and 700 °C the kinetics were found to decrease with increasing temperature due to the formation of the viscous glass. These results suggest that for a complete reduction in industrial process, the formation of the viscous glassy state should be avoided.

<https://doi.org/10.1007/s11663-023-02889-z>  
© The Author(s) 2023

## I. INTRODUCTION

THERE has been a push on decarbonization of metallurgical processes including for non-ferrous systems such as in lead production from primary and secondary resources. The use of hydrogen, as reductant and fuel, is vital in this decarbonization effort. Nevertheless, the existing studies in the literatures on lead recovery from lead-bearing slag were mainly focused on the use of carbon-based reductant (*e.g.*, coke, methane); and of these, the processes were carried out mainly through a liquid state reduction.<sup>[1–4]</sup> In addition to the high carbon footprint, a carbothermic process is often resulting in the formation of metal carbide as by-product which provide more complexity. A solid-state reduction process with hydrogen as a reductant is appealing in terms of development of carbon neutral

process. The fundamental understanding on the solid-state reduction using hydrogen on multicomponent slag system is essential for effective valuable metals recovery and for industrial waste/by-product cleaning processes. Thus, the current work aims to provide a fundamental information to support the development of a low-carbon footprint technology to process solid wastes/by-products and at the same time recover the valuable metals.

Although the global primary lead production has been decreasing in the last decade, the general trend of total refined lead production is slowly increasing, as reported by the International Lead and Zinc Study Group (ILZSG).<sup>[5]</sup> The main reason is due the importance of lead metallurgy and its role in supporting circular economy and metals recycling, *i.e.*, lead and lead-containing slag are suitable medium/carrier for the recycling of various precious and strategic elements from secondary resources (waste PCB, batteries, *etc.*). This also re-emphasise the importance of the current study.

There are limited studies on the kinetics of lead recovery from lead oxide and lead-containing compounds using hydrogen in the literatures (in the context of metallurgical recycling). The existing studies on hydrogen reduction on lead-bearing slag system were mainly related to the hydrogen reduction of PbO–SiO<sub>2</sub> (lead silicate) glass in the context of glass industries.<sup>[6–8]</sup>

A. RUKINI, M.A. RHAMDHANI and G.A. BROOKS are with the Fluid and Process Dynamics Group, Swinburne University of Technology, Melbourne, VIC 3122, Australia. Contact e-mail: ARhamdhani@swin.edu.au A. VAN DEN BULCK and T. VAN ROMPAEY are with the Umicore Corporate Research and Development, 2250, Olen, Belgium.

Manuscript submitted March 4, 2023; accepted August 10, 2023.

Article published online August 22, 2023.

There have been studies of hydrogen reduction on lead silicate for glass application of electron multiplier devices,<sup>[9]</sup> X-ray shield (XRS) glass,<sup>[6]</sup> and microchannel plates.<sup>[7,8]</sup> Hydrogen reduction was reported as an essential treatment in the fabrication of typical lead silicate glass to generate a conductive layer on a microchannel plate glass<sup>[7]</sup> and to develop glass resistivity for a typical X-ray shield (XRS) glass.<sup>[6]</sup> For those mentioned purposes, the hydrogen reduction on silicate glass have been studied at very low temperature within the solid-state reduction range to improve the glass' electrical and surface properties. Surface properties is an important aspect of glass which a certain textures and surface morphology gives a good channelling property. Following the solid-state reduction of lead silicate glass in hydrogen atmosphere, the glass typically subjected to annealing and devitrification.<sup>[10]</sup> Extensive studies on lead silicate glass were also found in the context of archeologic examination of historic glasses.<sup>[11,12]</sup> These studies focused on glass composition and structure identification, where correlations between glass vibrational parameters with composition were established.<sup>[13–16]</sup> These studies utilized characterization and optical techniques that are useful both for glass and slag studies. Through these studies, some of the lead silicate glass properties (*i.e.*, chemical, mechanical, thermal, vibrational spectra, optical *etc.*) have been investigated.

Pal *et al.*<sup>[17]</sup> reported a lead-silicate slag reduction with a focus on the investigating the relative contribution of reaction rates at different interfaces. They performed the hydrogen reduction on PbO-SiO<sub>2</sub> melts at 900 °C and evaluated the reduction rate at slag/gas, slag/refractory, and slag/metal interfaces. The reduction kinetics were evaluated through the measurements of mass loss and concentration profiles using electron microprobe. They reported that the reduction reaction was occurring at the slag/gas and slag/refractory interfaces, while the reaction at the slag/metal interface was quite negligible. They also reported that the reduction rate was decreasing with increasing amount of P<sub>2</sub>O<sub>5</sub> in the slag, which suggested a surface blocking mechanism by P<sub>2</sub>O<sub>5</sub> due to its surface-active nature.

The current study is part of a broader systematic study that is investigating the reduction and recovery of lead from lead-bearing oxides and slags using hydrogen at temperature ranges where solid-state reduction is expected. This involves a systematic experimental work of reduction of a simple unary PbO, binary PbO-SiO<sub>2</sub>, ternary/quaternary PbO systems, and finally to industrial complex PbO slags. In a previous paper by the authors,<sup>[18]</sup> a detailed kinetics study of PbO pellet reduction by hydrogen has been presented. The current study focuses on the hydrogen reduction of PbO-SiO<sub>2</sub> pellets at sub-liquidus temperature ranges. The kinetics and the mechanism of the reduction are investigated with the focus and context of extraction and recovery of lead from the material.

## II. EXPERIMENTAL PROCEDURES

### A. Slag/Glass Composition and Details of Pellet Making

In the current study, a lead silicate slag/glass with composition of 70 wt pct PbO and 30 wt pct SiO<sub>2</sub> (which corresponds to 38.6 mol pct PbO and 61.4 mol pct SiO<sub>2</sub>) was utilized. As can be seen from the binary phase diagram of PbO and SiO<sub>2</sub> presented in Figure 1 (constructed using FactSage 8.2 thermochemical package), this particular composition has a relatively low melting point of 732 °C. In addition to the low melting point, this composition was chosen because it represents a eutectic composition with highest amount of SiO<sub>2</sub> (~29.6 wt pct SiO<sub>2</sub>) compared to the other eutectic compositions (*e.g.*, 8.2 wt pct SiO<sub>2</sub> and 15.4 wt pct SiO<sub>2</sub>). The concentration of SiO<sub>2</sub> also resembles the typical industrial slag composition of 30 to 40 wt pct SiO<sub>2</sub>. Considering this composition, the expected phases at equilibrium at 600 °C and 700 °C are PbO-SiO<sub>2</sub> and SiO<sub>2</sub>; while at 500 °C are 3PbO-SiO<sub>2</sub> and SiO<sub>2</sub>; respectively.

This PbO-SiO<sub>2</sub> slag/glass was prepared by mixing both PbO (purity > 99.9 pct, sourced from Sigma Aldrich) and SiO<sub>2</sub> (purity > 99.8 pct, sourced from Alfa Aesar) powders in a ball mill for 24 hours. The corresponding mixed powders were then melted in an alumina crucible at 800 °C for 30 minutes before cast into a mould. The slag /glass was analysed using X-ray fluorescence (XRF) and X-ray diffraction (XRD) analyses which confirmed its composition and homogeneity. The XRD analysis result showed broad spectra which indicated that the material was in an amorphous/glass state after casting. The cast slag/glass was then crushed and sieved down to size 325 mesh (– 45 μm) before pelletized. Approximately 2.5 g of the PbO-SiO<sub>2</sub> powders were pressed in a steel die using a hydraulic pressing machine with 5 tonnes of force for 20 minutes to make pellets with an average diameter of 29.5 mm and thickness of 4.2 mm. The pelletizing process was resulting in pellets with apparent density of 871 kg/m<sup>3</sup>. Meanwhile, the theoretical density of a mixture of 70 wt pct PbO and 30 wt pct SiO<sub>2</sub> (which corresponds to 38.6 mol pct PbO and 61.4 mol pct SiO<sub>2</sub>), assuming a “rule of mixture”, is 4796 kg/m<sup>3</sup>.<sup>[16,19,20]</sup> This suggests that the pellets were quite porous.

### B. Hydrogen Reduction Set-Up

In this study, systematic microstructure investigation and kinetics analyses of solid state PbO-SiO<sub>2</sub> pellets reduction in a mixture of 15 pct hydrogen-85 pct nitrogen (H<sub>2</sub>/N<sub>2</sub>) atmosphere were carried out. The main reason of using a low hydrogen concentration in the gas mixture is for a safe laboratory experimental procedure (reduce flammability of the gas mixture). Different concentration of hydrogen in the gas mixture may affect the reduction kinetics, however, the

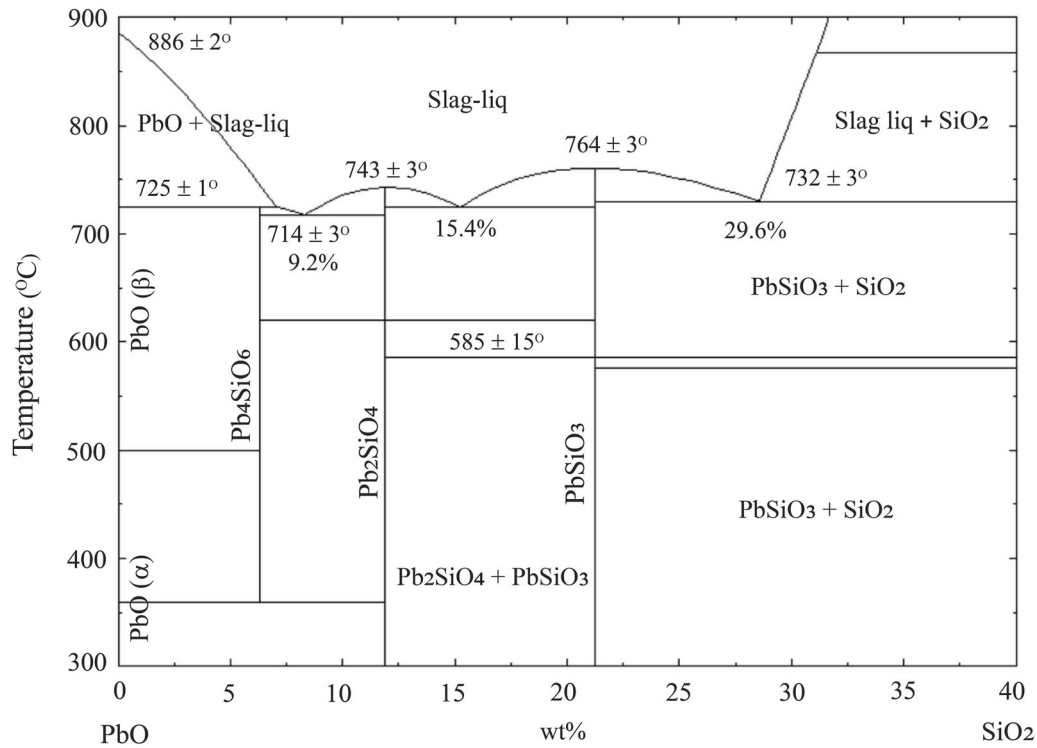


Fig. 1—Phase diagram of PbO–SiO<sub>2</sub> binary slag system constructed using FactSage 8.2 thermochemical package.

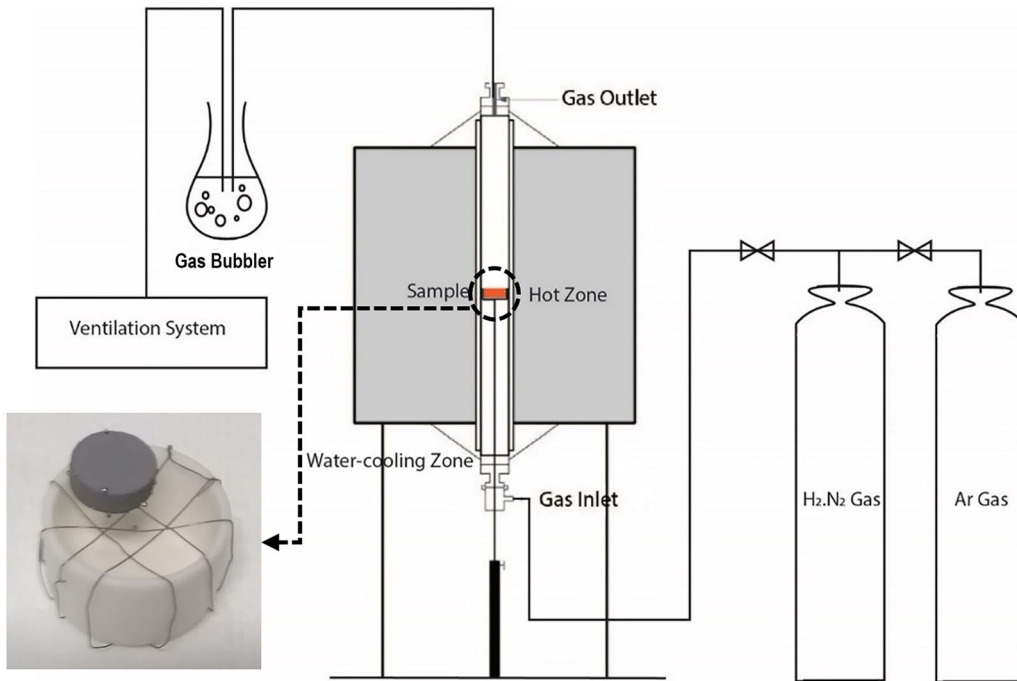


Fig. 2—A schematic of experimental apparatus consisting a vertical resistance tube furnace; with sample holder, gas and ventilation systems; (inset) a crucible holder system equipped consisting a shallow alumina crucible with Ni–Cr wire net to hold the pellet sample and functioning as a drain for liquid Pb. Reprinted from Ref. [18], under the terms of the Creative Commons Attribution 4.0 International License.

investigation of the effect of hydrogen concentration is beyond the current study. The mixture of ultra-high purity hydrogen and nitrogen gas was sourced from Coregas.

Isothermal reductions of PbO·SiO<sub>2</sub> pellets at temperatures between 300 °C and 800 °C were performed in an RHTV 120-300/18 Nabertherm vertical tube furnace (equipped with Mo<sub>2</sub>Si heating elements) using fixed bed

type of reactor (as shown in Figure 2). In anticipation of producing liquid Pb during the reduction, a special sample holder arrangement was adopted where a shallow crucible was equipped with nickel chromium wire net as shown in Figure 2 (inset). This would allow the sample to be suspended and readily react with the hydrogen in the atmosphere and at the same time let any possible lead liquid to drip down and contained within the crucible.

The temperature in the hot zone was calibrated using a standard reference thermocouple and provided an accuracy within  $\pm 1$  °C. The PbO–SiO<sub>2</sub> pellet was placed above the wire net on the crucible; and the whole system was positioned in the cool zone before the furnace was sealed and ultrahigh purity Argon was blown into the furnace chamber for 5 minutes to purge the air out. For the experiments, the furnace was then heated to the designated temperature before the H<sub>2</sub>/N<sub>2</sub> gas mixture was flown into the furnace chamber with constant gas flowrate of 500 mL/min. The pedestal was then lifted up to position the pellet and crucible system in the hot zone of the furnace and this was set to be the time zero for the reaction. The pellet was then let to react with the hydrogen in the gas for different reaction times (from 30 minutes to 3 hours). To terminate the reaction, the furnace chamber was bleed with Ar gas to flush the hydrogen mixture out of the furnace chamber, then the pedestal was lowered to position the pellet in the cooling zone (cooled by circulating water and cold Ar gas) and let to rest for 30 minutes before the sample was extracted out from the furnace. The PbO–SiO<sub>2</sub> pellet was then weighed after the reduction experiments and characterized.

### C. Characterizations and Kinetics

The surface morphology and cross section of the samples prior and after reduction were investigated using a scanning electron microscope (SEM), *i.e.*, SEM Zeiss Supra 40 VP, operated using 10 to 15 keV accelerating voltage. The SEM instrument was equipped with energy dispersive X-ray spectroscopy (EDS) detectors, in which elemental characterizations were also carried out. The phases analysis was carried out using XRD Bruker D8 Advance (Cu K $\alpha$ ,  $\lambda = 1.5418$  Å) with  $2\theta$  from 5 to 80 deg. Raman analysis was carried out for the purpose of studying the Q species in the silicate network. Raman spectra of lead silicate slag samples were collected at wavenumber range of 100 to 3200 cm<sup>-1</sup> using InVia Raman Spectroscope from Renishaw equipped with Leica microscope and used 514 nm laser type. CasaXPS software was used for peaks identification and deconvolution of the spectra.

The progress of kinetics of PbO–SiO<sub>2</sub> reduction by H<sub>2</sub>–N<sub>2</sub> gas mixture were tracked by measuring the mass loss of the pellets at particular time and temperature. The degree of reduction or extent of reduction at a particular time ( $\alpha_t$ ), defined as the ratio of mass loss measured at that time ( $\Delta W_t$ ) with theoretical maximum mass loss ( $\Delta W_{\text{total}}$ ), was calculated at different reaction time following Eq. [1]. Here,  $m_t$ ,  $m_i$  and  $m_f$  are the mass at time  $t$ , at initial and at time final, respectively. It was

assumed that the mass loss measured reflects the oxygen removal from PbO in PbO–SiO<sub>2</sub> glass/slag with neither substantial evaporation of raw material (PbO–SiO<sub>2</sub>) nor product (Pb). The final theoretical mass loss was defined as the total possible mass loss when all oxygen element is completely removed from PbO within the PbO–SiO<sub>2</sub> glass/slag.

$$\alpha_t = \frac{\Delta W_t}{\Delta W_{\text{total}}} = \frac{m_i - m_t}{m_i - m_{\text{total}}} \quad [1]$$

The incorporation of  $\alpha$  into a suitable model is useful for kinetics analysis and also to be used to determine the rate controlling step and micro-mechanism. Models that represent the solid-gas reaction have been comprehensively explained.<sup>[19–23]</sup> The current work kinetics interpretation includes the fitting of experimental result data ( $\alpha$ ) into existing isothermal kinetics models which include nucleation models, reaction order models, geometrical contraction models, and diffusion models. The value of ( $R^2$ ) from a linear regression of each model was evaluated and triangulated with the phase analysis and microstructure evolution observation to determine the micro-mechanism and possible rate limiting step.

## III. RESULTS AND DISCUSSION

### A. Macro- and Micro-Observations

Macro-observation of the lead silicate pellets post hydrogen reduction was carried out and the macro images of the samples are presented in Figure 3. It can be seen that there were colour and shape alterations with reduction time and temperature. The original colour of the pellet was white, and it was gradually changed into brownish and then blackish after reduction. It was clear that the hydrogen flow through the pellet pores resulted in the reduction of PbO within glass structure into Pb, and consequently altered the pellet colour from white to brownish then blackish as the reduction time was prolonged. This colour changing phenomena was also observed and reported by previous studies on hydrogen reduction of PbO-containing glass.<sup>[6,8]</sup>

In addition to the colour change, physical alterations of the pellets shape were also observed on samples reduced at 600 °C and above. This shape change appeared to occur due to sintering process and then followed by glass softening phenomenon experienced by the samples. Shrinkage due to sintering was able to be observed on samples reduced at 600 °C during 30 minutes to 1h reduction. As soon as the sample was sintered, the material was soften and tended to form a round shape due to its high surface tension. Figure 4 summarized the typical glass transition temperatures ( $T_g$ ) of a glass mixture with different SiO<sub>2</sub> concentration as reported by Kacem *et al.*<sup>[16]</sup> In Figure 4, the estimated composition changes of the PbO–SiO<sub>2</sub> samples reduced at different temperatures in the current study are also presented. It can be seen that samples with 30 wt pct of SiO<sub>2</sub> would start to experience glass softening at about 495 °C. The samples that were reduced at 500 °C were close to this softening region. However, as the PbO

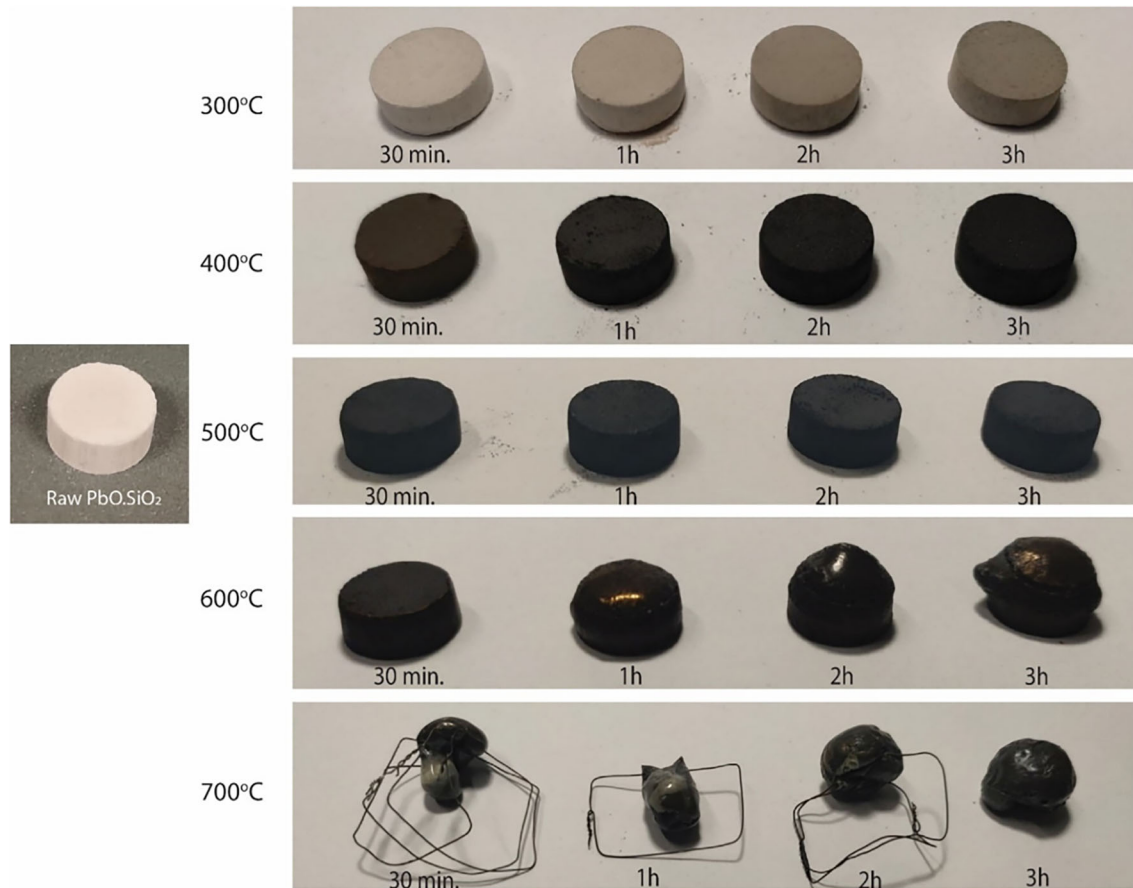


Fig. 3—Macrographs of lead silicate pellets prior (left) and post reductions (right) at temperatures 300 °C to 700 °C and times 30 min to 3 h in 15 pctH<sub>2</sub>-N<sub>2</sub> atmosphere.

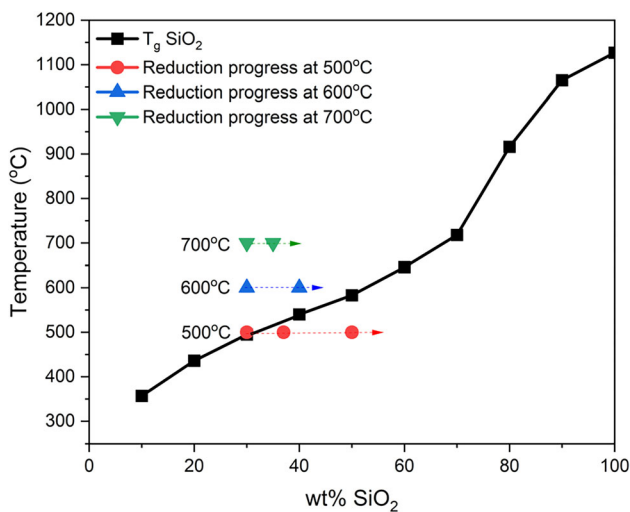


Fig. 4—Glass transition temperature ( $T_g$ ) as a function of wt pct SiO<sub>2</sub> and the expected SiO<sub>2</sub> concentration change of the pellets reduced at 500 °C, 600 °C, and 700 °C. Data of  $T_g$  was taken from Kacem *et al.*<sup>[16]</sup>

reduction kinetics were quite fast (will be discussed in the kinetics section in later section), the composition was quickly moving towards a higher SiO<sub>2</sub> concentration (red line in Figure 4) and brought the samples into a

region where the softening phenomenon is not occurring at 500 °C. On the other hand, in the case of reduction of samples at 600 °C and 700 °C (blue and green lines in Figure 4), the composition ranges of the samples were located above the glass transition temperatures, hence they experienced the softening phenomenon during the reduction process. These were clearly shown in Figure 3, where significant changes in pellet shape were observed in samples reduced at 600 °C and 700 °C.

The softening phenomenon occurs at the range of glass transition; where the glass will start to behave solid-like (for cooling down process) or transition from rigid state to flexible/rubbery state (for heating process) like in the case of the current study where solid pellet started to behave fluid-like during reduction above 500 °C. Shrivastava<sup>[22]</sup> described that softening occurs due to the increasing number of free volume (by about 2.5 times) in between silicate molecular chains. It should also be noted that glass transition does not involve a transition between thermodynamic states/phases (*e.g.*, solid vs liquid), because when this phenomenon happens, the silicate network within the glass become more viscous without any change in the materials structure. Rather, the glass has intramolecular covalent bonding broken allowing it to behave like fluid-like amorphous structure.<sup>[24,25]</sup> Therefore, even though the glass become viscous, *i.e.*, above  $T_g$ , it is not yet a liquid as it still

below the melting point ( $T_m$ ). Glass transition is a dynamic process where cooling or heating rate also heavily affect the phenomenon, in addition to the temperature. In the case of reductions of the PbO–SiO<sub>2</sub> pellets at 500 °C to 700 °C, clearly the mechanism of reduction was heavily affected by the softening phenomenon.

The cross section of the pellet sample reduced at 600 °C is shown in Figure 5. It can be seen that the sample underwent a reduction in the interior (as evidenced by the formation of Pb droplets) and at the same time it was slowly softened (accompanied by pellet shape change). It can also be seen from Figure 5 that micro bubbles were also observed in the interior of the sample. These micro bubbles appeared to form due to entrapped gas (H<sub>2</sub>–N<sub>2</sub>) as well as from the gas generated from the reduction reaction (H<sub>2</sub>O). At 700 °C, the samples were softened rapidly compared to that of at 600 °C. It appeared that this softening phenomenon and the formation of a viscous glass provided a barrier for reduction.

Figure 6 shows the cross section of the sample reduced at 700 °C. It can be seen from the Figure 6 that there was unreduced part of sample in the pellet's interior which was due to the viscous layer formed. Some pores/bubbles were also observed in the pellet's interior. It appeared that some of these bubbles had

coalesced forming much larger bubbles (compared to samples reduced at 600 °C) and a dome shape. Overall, the samples that were reduced above their glass transition temperature (reduced at 600 °C and 700 °C) had lower kinetics (will be described in the kinetics section) and that reduction process mainly happened at the region near the surface of the pellet. Figures 5(a) and (c), 6(a) and (c), show the formation of Pb micro-droplets on the top surface of the sample as well as under the dome/big bubbles in the interior.

The general schematic of the shape alteration sequence on the PbO–SiO<sub>2</sub> samples during hydrogen reduction below and above the glass softening point is illustrated in Figure 7. It can be seen from Figure 7 that for samples reduced at temperatures below the softening point, they were able retain the original pellet shape (no significant shape change). This is different compared to the samples reduced above the softening point. Above the softening point, the sample became soften and densification occurred. Overall, the shape alteration on the samples started by the softening phenomenon which resulted in some of the pellet part drooping down toward the crucible due to gravity. Due to the viscous nature of the materials, the part that was drooping did not really separate from main body of the pellet. As the softening uniformly occurred around the structure and that reduction proceeded, some gas was trapped within

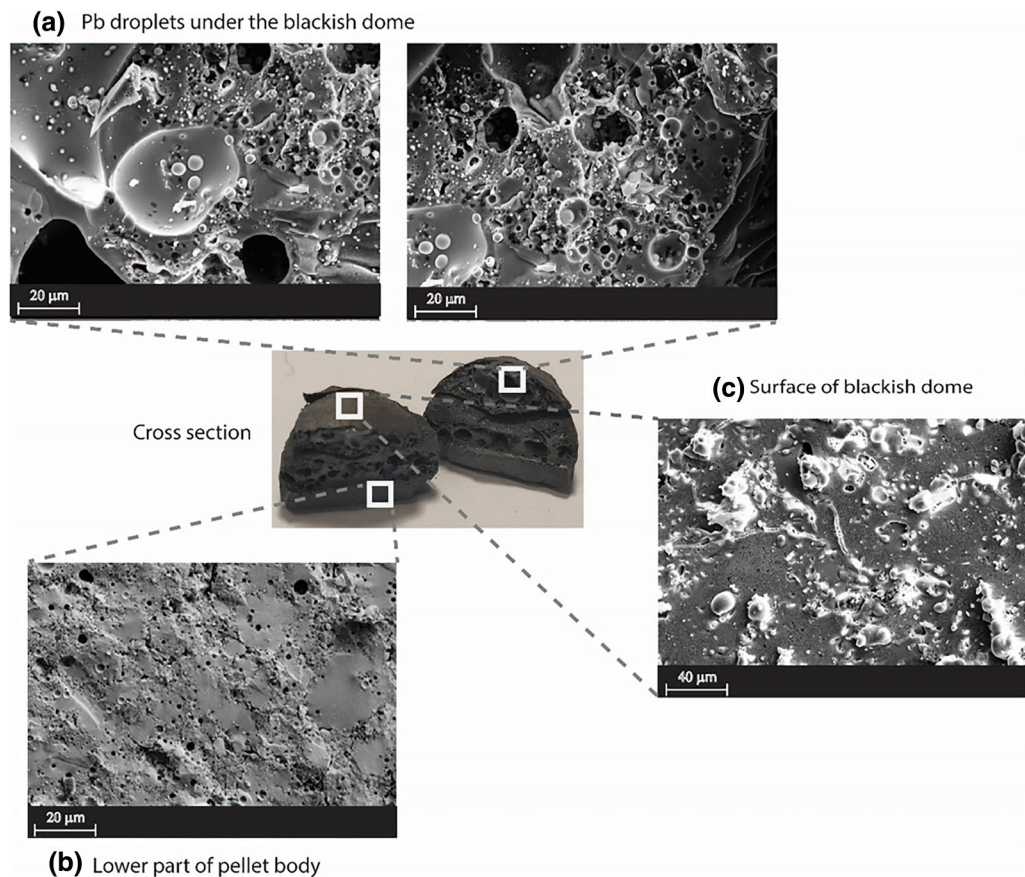


Fig. 5—SEM images of lead silicate pellet surface and cross-section post reduction at 600 °C reduced for 2 h in 15 pctH<sub>2</sub>–N<sub>2</sub> atmosphere, showing: (a) Pb droplets under the dome, (b) dense area at the bottom of pellet, (c) surface of the dome.

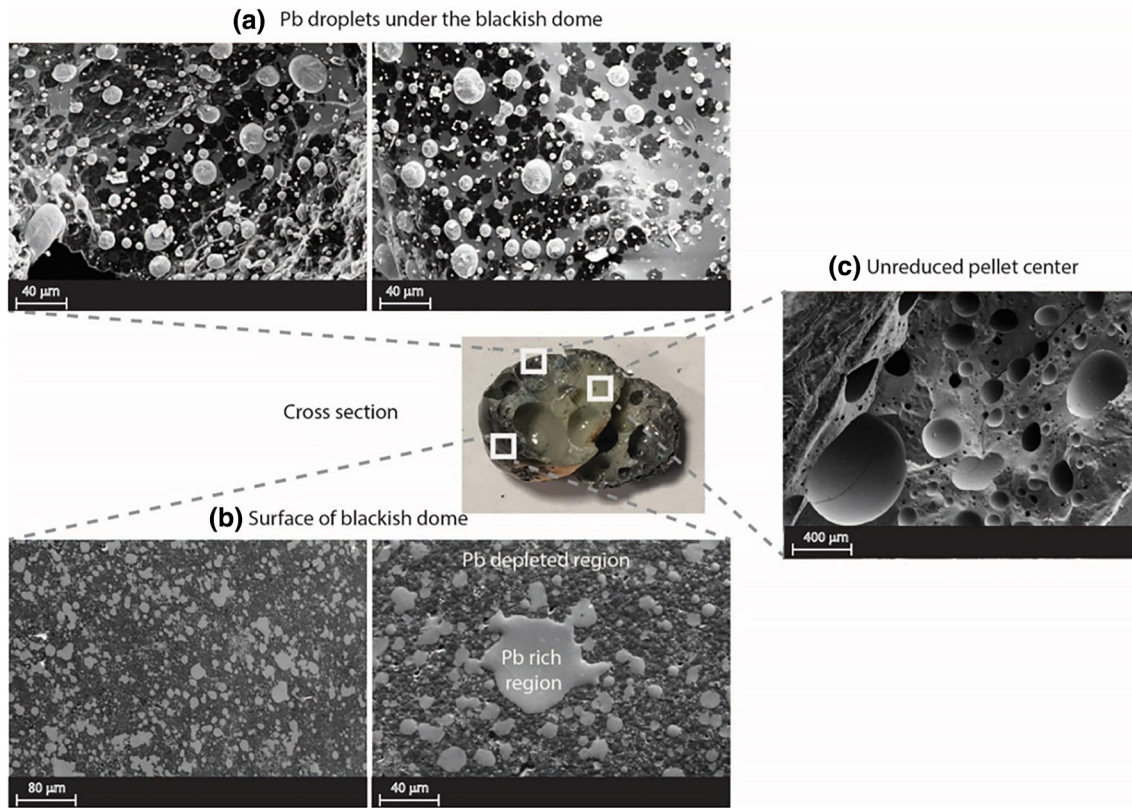


Fig. 6—SEM images of lead silicate pellet surface and cross-section post reduction at 700 °C reduced for 2 h in 15 pctH<sub>2</sub>-N<sub>2</sub> atmosphere, showing: (a) Pb droplets under the dome, (b) surface of the dome, and (c) unreduced pellet center.

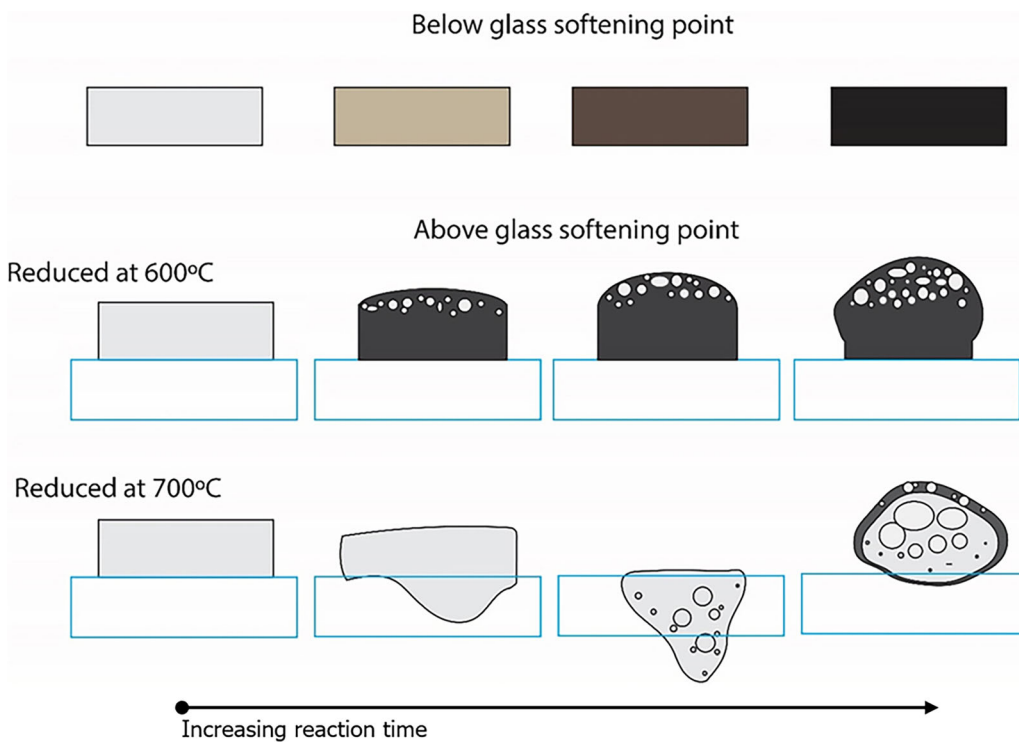


Fig. 7—An illustration of the cross section and surface appearance of PbO-SiO<sub>2</sub> pellet after reduction in 15 pctH<sub>2</sub>-N<sub>2</sub> atmosphere at different temperatures (below and above glass transition softening point) and reaction times.

the pellet forming bubbles (as can be seen from Figures 5 and 6). The final stage of the shape alteration included the formation of a bloated round shape sample, which might have indicated that the highly viscous melt had a high surface tension and it tended to shape into a single big droplet to reduce its overall surface energy.

### B. Semi-quantitative EDS Analysis

Selected semi-quantitative EDS point analyses were carried out on parts of the reduced pellet samples at 700 °C, and the results are presented in Table I and Figure 8. The original composition of raw lead silicate pellets in this study was 70 wt pct PbO and 30 wt pct SiO<sub>2</sub> in which the breakdown of weight percent of elements is also given in Table I. The total initial amount of Pb was 65 wt pct and while the total oxygen from both PbO and SiO<sub>2</sub> was 21 wt pct. EDS analysis on the unreduced interior part of the sample reduced at 700 °C (Figure 6(c)) revealed that it contains fairly similar composition to the initial lead silicate pellet composition. The microdroplets formed under the blackish dome (Figure 6(a)) was also confirmed to be Pb (as shown in Table I). The lead-rich region (light grey area) on the surface of the dome (Figure 6(b)) showed a relatively high Pb concentration that only get about 2 pct decrease of Pb compared to the Pb concentration in the initial pellet. This light grey area appeared to be a Pb pool on a partially reduced PbO-SiO<sub>2</sub> surface, indicated by the low concentration of oxygen. The lead-depleted regions (dark grey areas in Figure 6(b)) both on the surface of the dome (outside) and under the dome (inside) showed only small concentration of lead (Table I). It appeared that this area was a SiO<sub>2</sub> phase.

Therefore, it appeared that upon heating at 700 °C in hydrogen atmosphere, the original glassy amorphous pellet underwent some transformation towards the formation of PbO-SiO<sub>2</sub> and SiO<sub>2</sub> phases (see phase diagram in Figure 1) at the same time of the formation of Pb droplets (mainly from the light grey phase); and these occurred majority on top part area of the pellet (as evidenced by Pb droplets on the dome). Zhang *et al.*<sup>[8]</sup> reported that lead that was produced by hydrogen reduction of Pb glass tends to form 'land' or aggregated Pb (similar to that shown in Figure 6(c)). In more detailed observations, the lead-rich regions (light grey phase) shown under the dome (in Figure 6(a)) were also the spots where the Pb droplets emerged from. In contrast with the previous study by the authors<sup>[18]</sup> on PbO pellet reduction by hydrogen which reported non-wetting Pb droplets formation on the surface of PbO, the Pb formed on the surface of the sample in the current study were quite wetting the top surface of PbO-SiO<sub>2</sub> or SiO<sub>2</sub> phases (Figure 6(c)). The wetting behaviour of the lead droplet will depend on a number of factors such as surface roughness, chemical heterogeneity of the surface (*e.g.*, type of bonding at the surface), and the force balance at the solid, liquid, gas interface; among others. The presence of SiO<sub>2</sub> appeared to provide a different intermolecular interaction at the liquid Pb and solid PbO-SiO<sub>2</sub> (or SiO<sub>2</sub>) interfaces resulting in low wettability compared to Pb-PbO

interface. It should be noted that the Pb droplets that were observed hanging under the dome exhibited almost a fully round shape due to the action of gravity.

### C. XRD and Raman Analyses

#### 1. XRD analyses results

The XRD analyses results on selected lead silicate samples prior and post reduction are given in Figure 9. The XRD spectra of the original lead silicate pellet sample (prior to reduction) showed typical spectra for an amorphous glass phase indicated by broad bumps (Figure 9 bottom). This result implied that the sample was initially amorphous prior to the reduction process. The sample reduced at 300 °C for 2 hours showed an early reduction process indicated by a colour change into brownish colour (Figure 3). However, the XRD spectra of this particular sample did not show any significant peaks, rather, similar spectra to the original materials (amorphous state) were observed. It appeared that this early stage of reduction resulted only a very small amount of lead and virtually the peaks were not visible on the XRD spectra. It should be noted that there was noticeable weight change observed at this temperature and reduction time indicated that reduction had occurred. This will be discussed in more detailed in the kinetics section.

Broad Pb XRD peaks were observed in the sample reduced at 400 °C for 2 hours. The broad peaks may indicate that the formed Pb were very fine at this condition. The Pb XRD peaks started to emerge and visible on sample reduced at 400 °C for 2 hours. The intensity of Pb peaks became significantly sharper and higher as the reduction temperature was increased to 500 °C and 600 °C. The sample reduced at 600 °C showed sharp and high lead peaks as early as 30 minutes of reduction time. At this time the pellet shape was still intact, however, as the reduction time was increased (for example to 2 hours), the pellet was significantly deformed due to the softening phenomenon. Beyond 30 minutes, it appeared that the reduction did not increase significantly due to the softening phenomenon and unreduced core. This was also confirmed by the calculated reduction conversion (will be discussed in the kinetics section).

A lower amount of lead (based on the XRD results) was observed in the sample reduced at 700 °C, this happened due to the faster softening phenomenon that already occurred at the early reduction time. The softening of the pellet resulted in a viscous layer that provide barrier and limit the reduction to only at the outer part of sample. This phenomenon was reflected on the XRD peaks of sample reduced at 700 °C where the outer part (part-b) showed higher amount of lead compared to that of the inner part of the sample (part-a). This was also supported by the reduction conversion of samples reduced at 700 °C being lowered than that reduced at 600 °C (will be discussed in the kinetics section). In addition, the XRD analysis of the part-a showed that it still had amorphous structure. It implied that the softening process in the current



**Table I. EDS Analyses Results of Selected Areas on the Lead Silicate Pellets Reduced at 700°C Shown in Fig. 6**

| Element | Original Composition of Lead Silicate Pellet |                 | Unreduced Part in the Sample's Interior |           | Lead Droplets Under the Dome |           | Lead-Rich Region |           |
|---------|--|-----------------|---|-----------|------------------------------|-----------|------------------|-----------|
|         | (Wt Pct)                                     | (At. Pct)       | (Wt Pct)                                | (At. Pct) | (Wt Pct)                     | (At. Pct) | (Wt Pct)         | (At. Pct) |
| Pb      | 65   | 15              | 64.71                                   | 15.41     | 100                          | 100       | 62.88            | 14.76     |
| Si      | 14   | 35              | 18.26                                   | 32.08     | —                            | —         | 21.09            | 36.52     |
| O       | 21 <sup>a</sup>                              | 50 <sup>b</sup> | 17.03                                   | 52.51     | —                            | —         | 16.02            | 48.71     |

| Element | Lead-Depleted Region (Inside) |           | Lead-Depleted Region (Outside) |           |
|---------|-------------------------------|-----------|--------------------------------|-----------|
|         | (Wt Pct)                      | (At. Pct) | (Wt Pct)                       | (At. Pct) |
| Pb      | 5.89                          | 0.60      | 8.46                           | 0.97      |
| Si      | 44.83                         | 33.93     | 58.47                          | 49.69     |
| O       | 49.28                         | 65.47     | 33.07                          | 49.33     |

<sup>a</sup>O (from PbO) = 5 wt pct and O<sub>2</sub> (from SiO<sub>2</sub>) = 16 wt pct.  
<sup>b</sup>O (from PbO) = 15 at. pct and O<sub>2</sub> (from SiO<sub>2</sub>) = 35 at. pct.

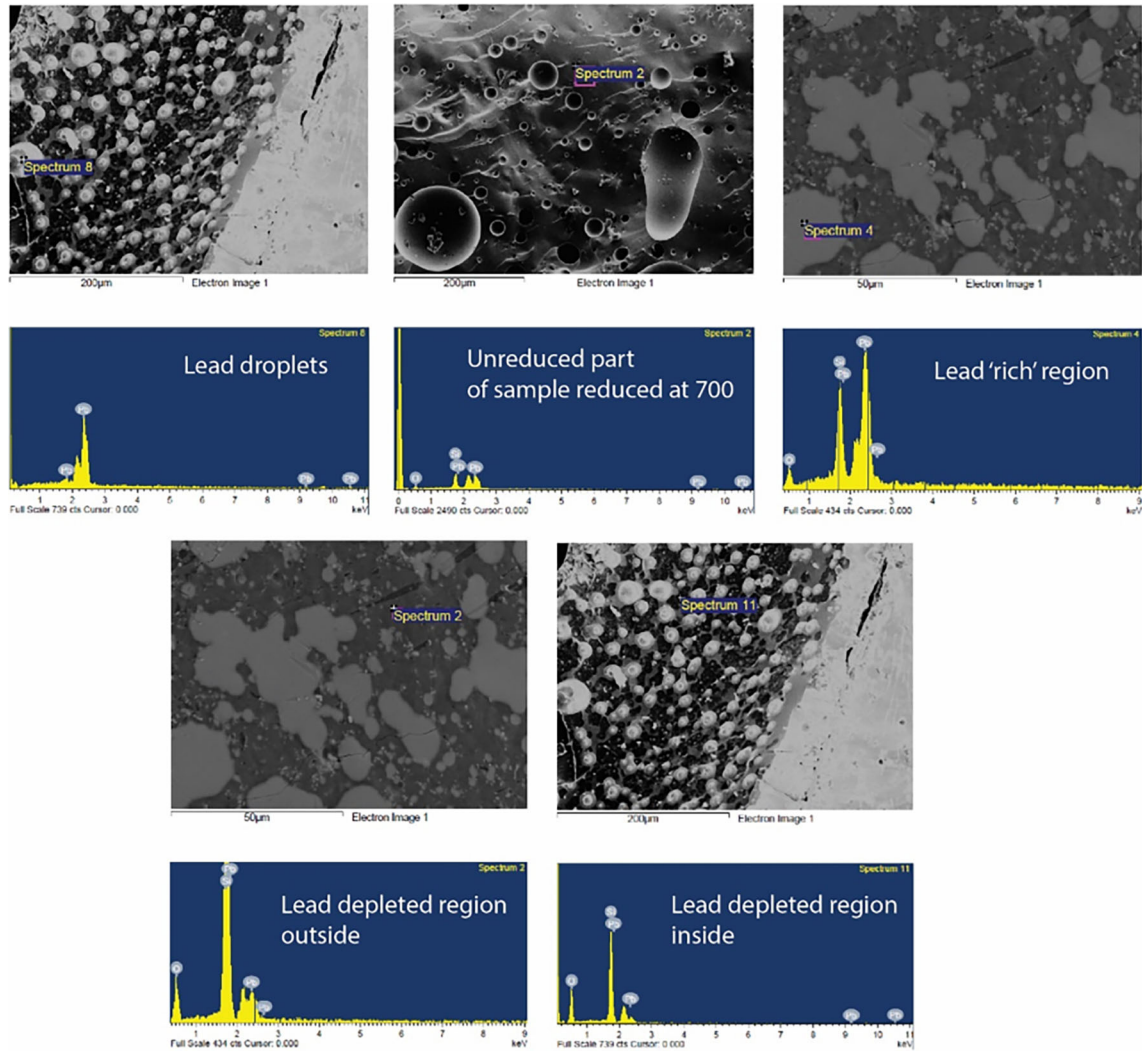


Fig. 8—EDS semi-quantitative analyses of selected areas on the reduced lead silicate pellets in 15 pctH<sub>2</sub>-N<sub>2</sub> atmosphere at 700 °C.

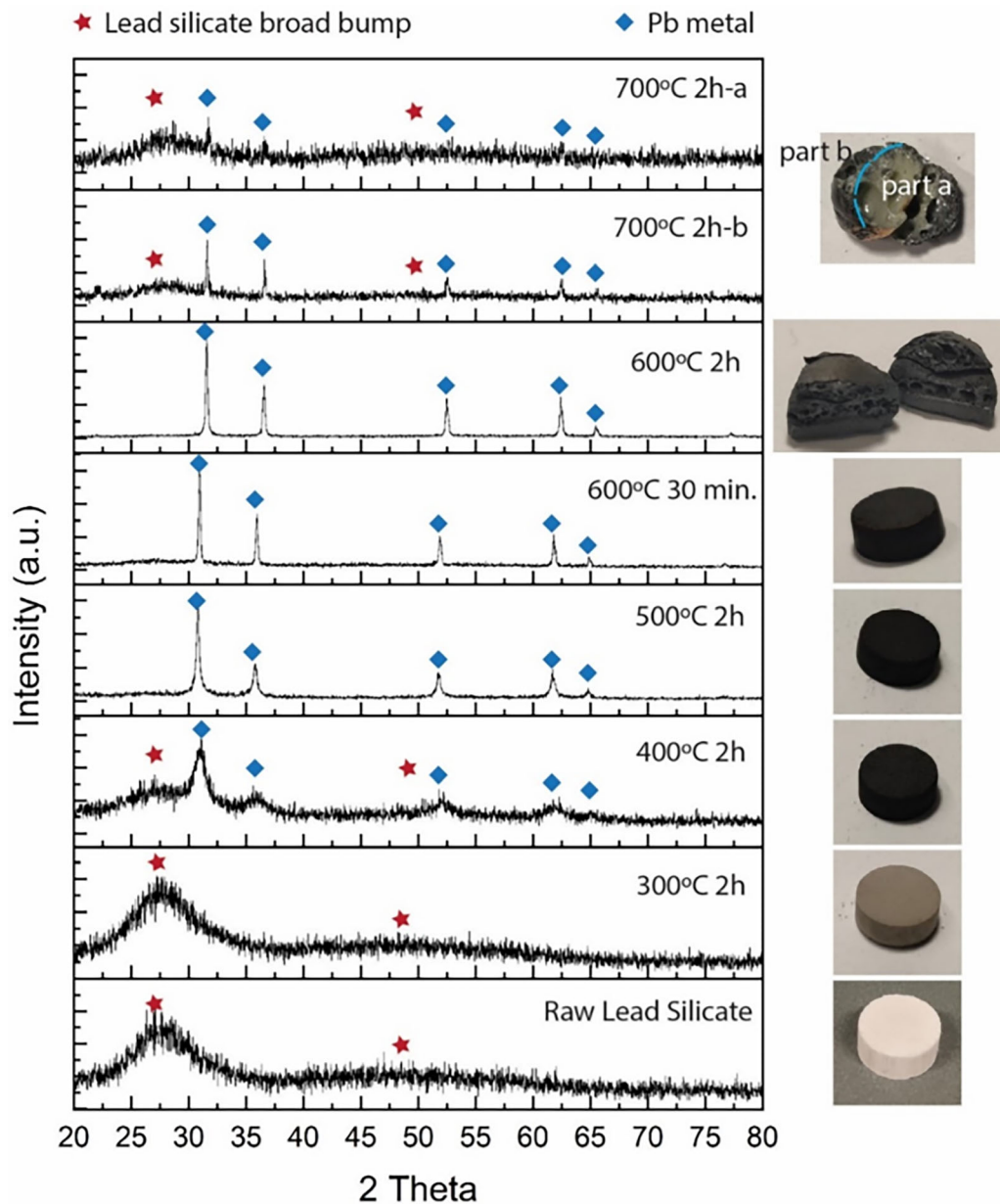


Fig. 9—Bulk surface XRD analyses (along with images reference) of the green pellet and the pellets reduced at 300 °C, 400 °C, 500 °C, 600 °C, and 700 °C for 2 h in 15 pctH<sub>2</sub>-N<sub>2</sub> atmosphere.

lead-silicate sample changed its viscosity but did not change the silicate network from amorphous into crystalline.

### 2. Raman spectroscopy analyses

Raman spectroscopy analyses were carried on the samples prior and after the reduction. The main purpose for the Raman spectroscopy analyses in the current study was to investigate the alteration of the silicate chains/species in the silicate network structure within the samples, before and after reduction. Typical silicate glass mainly built by silicate species that share oxygen to their adjacent silicate species and forms a silicate network; which shown schematically in Figure 10. There are several classifications of bonding based on the

number of bridging oxygen (BO) and non-bridging oxygen (NBO) made by the silicate network. An isolated simple silicate that makes no bonding to other silicate is called  $Q^0$ ; when two silicates share one of their oxygens and forms a smallest unit of  $Si_2O_7$ , it is called  $Q^1$ ; if the tetrahedra silicates share their two and three of the oxygens with the nearest adjacent silicate, they will make  $Q^2$  and  $Q^3$  bonding type, respectively. Silica species where all of their oxygens are connected with other silica species form  $Q^4$  bonding. PbO is categorized as an amphoteric oxide where the structural role of PbO in a silicate glass is concentration dependent. At low PbO content, less than 40 mol pct PbO, Pb was reported to present as a network modifier that connected to silicate network,<sup>[9,10,14]</sup> while above this concentration Pb will

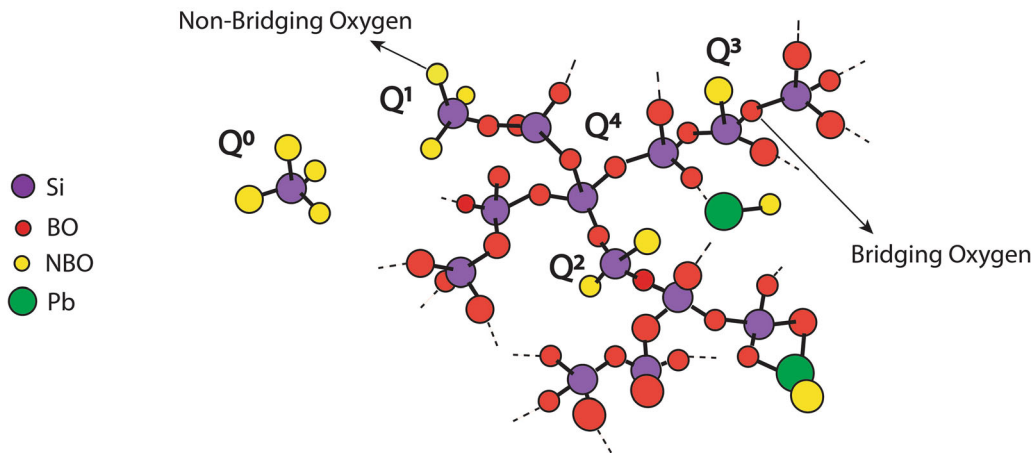


Fig. 10—Lead silicate network illustration depicting the bridging oxygen, non-bridging oxygen bonding and  $Q$  species.

Table II. Raman Spectra of PbO Stretch and Silicate Species

| Wavenumber ( $\text{cm}^{-1}$ ) | Network Type/Species | References   |
|---------------------------------|----------------------|--|
| 135–140                         | Pb–O stretching      | Filho <i>et al.</i> , <sup>[26]</sup> Furukawa <i>et al.</i> <sup>[15]</sup> |
| 300–600                         | Si–O–Si bending      | Robinet <i>et al.</i> <sup>[11]</sup>  |
| 900–1300                        | Si–O stretching      | Robinet <i>et al.</i> <sup>[11]</sup>  |
| 850–870                         | $Q^0$                | Mysen <sup>[27]</sup>  |
| 905–920                         | $Q^1$                | Mysen <sup>[27]</sup>  |
| 950–970                         | $Q^2$                | Mysen <sup>[27]</sup>  |
| 1050–1100                       | $Q^3$                | Mysen <sup>[27]</sup>  |
| 1065                            | $Q^4$                | Mysen <sup>[27]</sup>  |

start to act as a network former. Wang *et al.*<sup>[9]</sup> reported that at PbO concentration less than 40 mol pct, the ionic bonding of PbO dominates which results in its behaviour as a network modifier; while above 40 mol pct, the Pb starts to be polarized and develop covalent bonds which makes it into a network former. Robinet *et al.*,<sup>[11]</sup> however, reported that at concentration of 35 to 40 mol pct PbO, the PbO already started to take over the role of a network former. However, the network within the glass remained stable and not depolymerized at this concentration. In the current study, the concentration of the PbO in the initial sample was 38.6 mol pct. It was pre-assumed that the PbO would act as silicate network modifier, and the presence of PbO in the sample would increase the NBO.

Table II shows a summary of the relevant wavenumber range for different  $Q^n$ , Pb–O stretching, Si–O stretching, and Si–O bending obtained from previous literatures. Figure 11 shows the results of the Raman spectroscopy analyses from the samples prior and after reduction for 30 minutes at different temperatures. One of the ways to evaluate the effect of PbO reduction on the silicate network is by evaluating the intensity of the Si–O–Si bending at  $\sim 500 \text{ cm}^{-1}$  and Si–O stretching at 900 to 1300  $\text{cm}^{-1}$ . It appeared that when reduction proceeded and more Pb droplets produced (reduced out from the sample), those peaks intensity were decreasing. It can be seen from Figure 11 that as the temperature

was increased from 300 °C to 400 °C the Raman spectra exhibited more noise; and there were decreasing intensity of the peaks mentioned. At 30 minutes reduction at these temperatures, fine Pb droplets were forming on the surface and appeared to start to break down the silicate network. At 30 minutes of reduction at 500 °C and 600 °C, extensive Pb formation and breakdown of silicate network had occurred; which resulted in the highly noise spectra in such that the silicate spectra were not visible anymore. At 700 °C there was significant softening of the sample which resulted in low reduction (low formation of Pb) at the center of sample, hence clear silicate spectra were detected. This study was also observed decreasing PbO peaks (at  $\sim 100$  to 150  $\text{cm}^{-1}$ ) post hydrogen reduction which confirms the reduction of PbO within the lead silicate glass.

One can estimate the relative fraction of each type of ( $Q^n$ ) bonding in the silicate network by carrying out deconvolution of the peak of Si–O stretching at 900 to 1300  $\text{cm}^{-1}$ , considering the specific  $Q^n$  wavenumbers in Table II. Due to faint Si–O stretch on samples that produced higher amount of lead, deconvolution of the Si–O stretch was only performed on spectra from samples prior and after reduction at 300 °C and 400 °C, in which the results are presented in Figure 12. The  $Q^n$  species fraction (in percentage) resulted from the deconvolution of samples reduced at 300 °C and 400 °C are tabulated in Table III. There are several quantitative

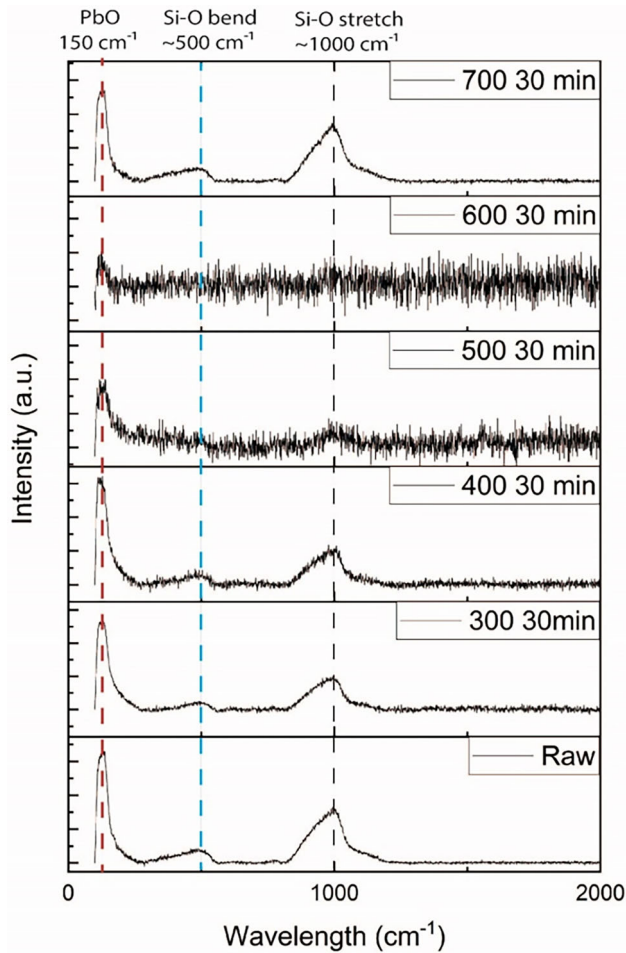


Fig. 11—Selected Raman spectra of lead silicate glass before and after reduction for 30 min at 300 °C, 400 °C, 500 °C, 600 °C and 700 °C in 15 pctH<sub>2</sub>-N<sub>2</sub> atmosphere.

parameters that can be used to describe the silicate network (*e.g.*, degree of polymerisation, NBO per tetragonal unit (NBO/T), *etc.*). The current study attempted to characterise the silicate network of the samples by evaluating the degree of polymerisation (DoP) and the number of NBO/T on samples reduced at 300 °C and 400 °C using formulation given in Eqs. [2] and [3],[28] respectively. It should be noted there have been a number of parameters used by previous researchers to represent the DoP, such as  $Q_3/Q_2$ ,  $(Q_3/Q_2)^2$ ,  $(Q^3 + Q^4)/(Q^0 + Q^1)$ ,  $Q^3/(Q^1 + Q^2)$ , as well as the NBO/T.[27–33]

$$\text{DoP}(Q^4) \approx \frac{Q^3}{Q^2} \text{ or } \left(\frac{Q^3}{Q^2}\right)^2 \text{ or } \left(\frac{Q^3 + Q^4}{Q^0 + Q^1}\right) \text{ or } \left(\frac{Q^3}{Q^1 + Q^2}\right) \quad [2]$$

$$\frac{\text{NBO}}{T} = (Q^0 \times 4) + (Q^1 \times 3) + (Q^2 \times 2) + (Q^3 \times 1) + (Q^4 \times 0) \quad [3]$$

One would expect an inverse proportionality between the NBO/T with the DoP. The different parameters of DoP (expressed in Eq. [2]) were calculated and the trend was compared to the NBO/T. It was found that the DoP parameter of  $(Q^3 + Q^4)/(Q^0 + Q^1)$  fit well with the inverse trend of the NBO/T. The results of the calculated DoP  $(Q^3 + Q^4)/(Q^0 + Q^1)$  and NBO/T, as well as the shift of  $Q^3$  are presented in the Table IV. It can be seen from the data in the Table that there is no clear trend between the  $(Q^3 + Q^4)/(Q^0 + Q^1)$  with the PbO reduction over time. Robinet *et al.*[11] reported that the change in PbO concentration in the glass would significantly shift the position of  $Q^3$  species in the Raman spectra, *i.e.*, the  $Q^3$  peak at around 1040 to 1070 cm<sup>-1</sup> would shift to lower wavelength with increasing Pb concentration. Similar trend was also observed in the current study which can be seen in Figure 12 (top right) and Table III, that shows the shift of the  $Q^3$  to a lower wavelength as the reduction proceed at 300°C and 400°C.

#### D. Kinetics Analyses and Calculation of Activation Energy

The overall degree of reduction ( $\alpha$ ) as a function of time of the PbO-SiO<sub>2</sub> pellet samples reduced in hydrogen atmosphere at 300 °C to 700 °C are presented in Figure 13. The values of degree of reduction were calculated considering the samples' mass change post hydrogen reduction using Eq. [1]. In general, the reduction degree was observed to increase with increasing reduction time. In the case of reduction at 300 °C, there was a significant increase in the reduction degree up to 25 minutes; beyond this time, further increase of reduction degree was sluggish. It was observed that there is an increase in the reduction degree with increasing reduction temperature from 300 °C to 500 °C (Figure 13(a)) with reduction degree increase from 7 to 47 pct at 3 hours of reduction, respectively. However, when the reduction temperature was increased above 500 °C, the overall reduction degree was found to decrease with increasing temperature (from 500 °C to 700 °C), as shown in Figure 13(b).

As has been discussed in the previous Section III-A, the softening phenomenon occurred extensively at temperatures above 500 °C. The decrease in the reduction degree above 500 °C appeared to be associated with the shrinkage and the formation of viscous phase that hindering reduction process. The viscous phase formation presumably affected the diffusion of either hydrogen gas and/or H<sub>2</sub>O product to/from the interior of the samples that reduced at 500 °C to 700 °C. The cross-section observation (Figure 6) on sample reduced at 700 °C showed that the interior of the sample was secluded with viscous structure and that reduction only occurred on the near surface; and the centre part of the pellet was confirmed to be unreduced from the EDS and XRD analyses. It also appeared that the softening phenomenon occurred more extensively on sampled reduced at 700 °C compared to that reduced at 600 °C. Hence, the samples reduced at 600 °C exhibited slightly higher reduction degrees.

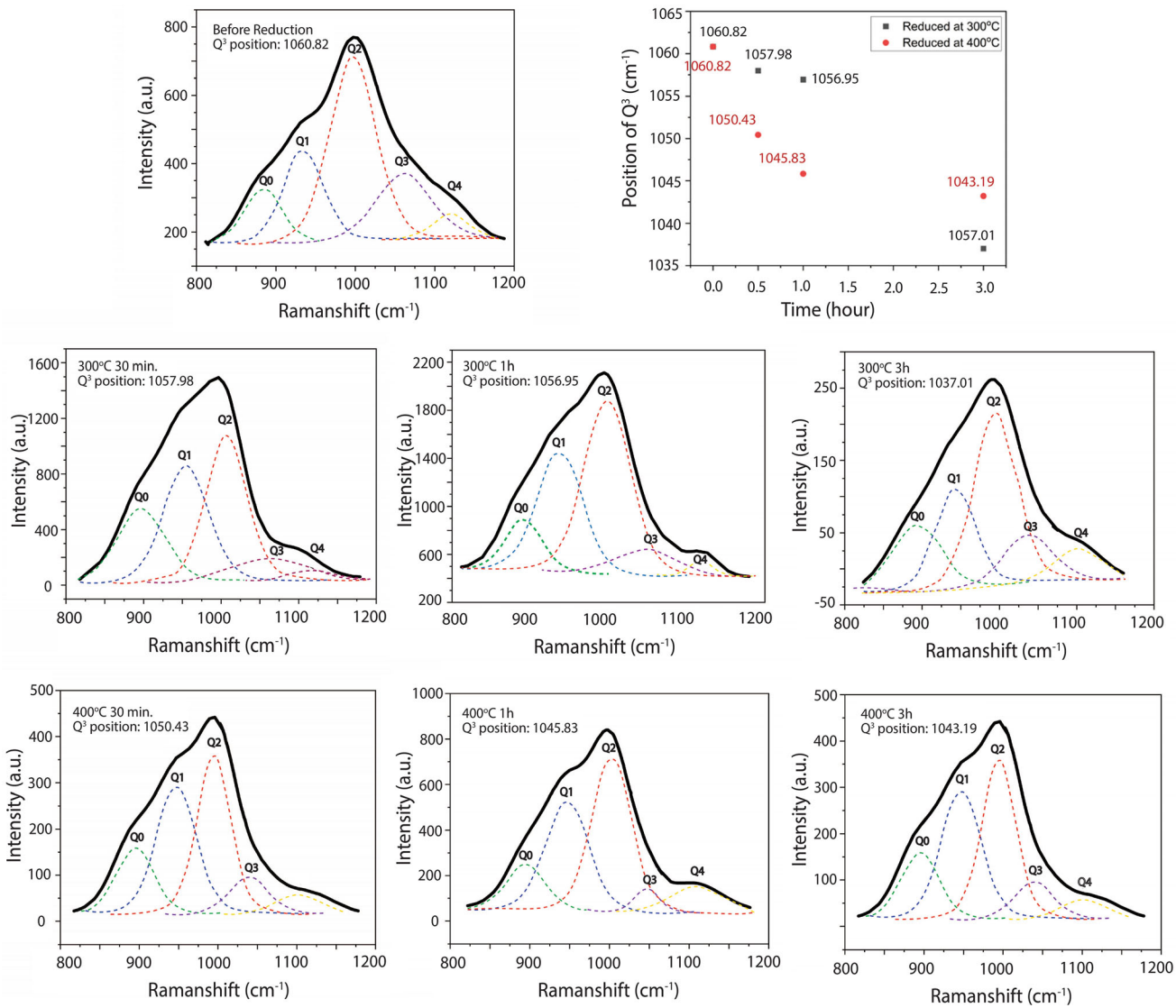


Fig. 12—Deconvolution of Raman spectra of samples reduced at 300 and 400°C and the correlation of  $Q^3$  position with reduction time.

**Table III.  $Q^n$  Species Fraction (in Percentage) of Samples Reduced at 300 °C and 400 °C**

| Sample           |                    | $Q^0$ (Pct) | $Q^1$ (Pct) | $Q^2$ (Pct) | $Q^3$ (Pct) | $Q^4$ (Pct) | Total (Pct) |
|------------------|--------------------|-------------|-------------|-------------|-------------|-------------|-------------|
| Temperature (°C) | Reduction Time (h) |             |             |             |             |             |             |
| 300              | 0                  | 11.06       | 19.63       | 44.98       | 19.51       | 4.82        | 100         |
|                  | 0.5                | 21.05       | 30.65       | 36.06       | 9.79        | 2.45        | 100         |
|                  | 1                  | 10.86       | 30.62       | 46.38       | 9.82        | 2.32        | 100         |
|                  | 3                  | 17.95       | 21.93       | 39.36       | 12.29       | 8.47        | 100         |
| 400              | 0                  | 11.06       | 19.63       | 44.98       | 19.51       | 4.82        | 100         |
|                  | 0.5                | 16.29       | 33.35       | 35.09       | 9.61        | 5.66        | 100         |
|                  | 1                  | 11.80       | 32.21       | 41.15       | 4.67        | 10.17       | 100         |
|                  | 3                  | 4.16        | 39.54       | 43.18       | 10.71       | 2.41        | 100         |

To evaluate the reduction degree more quantitatively, the data obtained from the experimental works were fitted into existing possible kinetic models of solid state reduction, *i.e.*, nucleation model (A), geometry model

(R), diffusion model (D). The models evaluation involved the use of conversion ( $\alpha$ ) data into the model equations to obtain  $k$  (constant rate) and  $R^2$  value from fitting of the data. Table V summarizes the results of the

calculations. It can be seen from Table V that the D1 (one-dimensional diffusion) and D2 (two-dimensional diffusion) models provide similar high  $R^2$  to the D3 (Jander) and D4 (Ginstling–Brouhnstein) models. The D1 and D2 representing diffusion processes in simplified one- and two-dimensional cases. To provide a more comprehensive kinetics evaluation that representing the actual sample shape (pellet), only 3D diffusion models of D3 and D4 were further evaluated.

The reduction degree data can be fitted really well to the diffusion models D3 (Jander) and D4 [Ginstling–Brouhnstein (GB)] with  $R^2$  value of each diffusion model ranges from 91 to 99 pct (underlined and bold texts in Table V). The differences between the  $R^2$  of the Jander and GB models are negligible, hence both are suitable to be used for analysing the reduction kinetics in the current study.

The Jander model basic formulation is shown in Eq. [4]. For a 3D sphere particle, the equation can be written as function of time as shown in Eq. [5]. The Jander 3D-model is also applicable for other shapes such as cylindrical pellet.<sup>[34]</sup> Jander model assumes negligible volume and density change during the reaction, hence more accurate for a case with low reduction degree (extent of reaction).<sup>[10]</sup> The Ginstling–Brouhnstein (GB) model, on the other hand, is an improvement of Jander model with a correction to the assumptions made and presented in Eq. [6].

$$x = R[1 - (1 - \alpha)^{\frac{1}{3}}] \quad [4]$$

$$kt = [1 - (1 - \alpha)^{\frac{1}{3}}]^2 \quad [5]$$

$$kt = 1 - \frac{2\alpha}{3} - (1 - \alpha)^2 \quad [6]$$

$$k = A \exp\left(-\frac{E_a}{RT}\right) \quad [7]$$

As can be seen in Table III, both Jander and GB models showed similar values of  $R^2$ . However, by looking at the dimension of the reduced PbO–SiO<sub>2</sub> samples, no significant size changes were observed upon reduction, except for samples reduced at 600 °C and 700 °C. The highest reduction degree was observed on samples reduced at 500 °C, *i.e.*, less than 50 pct at 3 hours of reduction, which could still be considered as having a low reduction degree. The samples reduced at 600 °C and 700 °C experienced significant shape change but the reduction degree was even smaller. Considering all of these, the Jander model was then selected to represent further the kinetics analyses and for the calculation of the activation energy ( $E_a$ ).

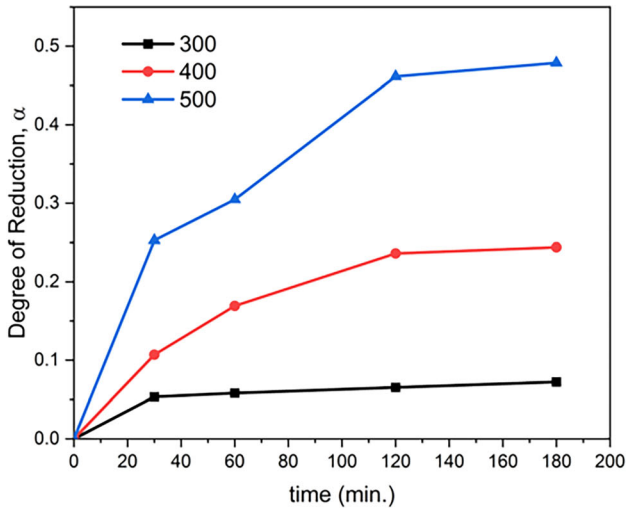
The plot of the kinetics data using the Jander model is presented in Figure 14. It can be seen from the figure that the data can be reasonably fitted into straight lines in which the  $k$  (rate constant) can be calculated. Once the  $k$  were calculated, an Arrhenius plot of  $\ln k$  as function of  $1/T$  was then constructed (using Eq. [7]) and shown in Figure 15. It can be seen from the figure that there are two kinetics regions. The Region I, with a range of temperature 300 °C to 500 °C, showed an increase of rate constant with increasing temperature. The associated activation energy for this Region I was calculated to be 70.7 kJ/mol. It was reported by Welter *et al.*<sup>[35]</sup> that the diffusion activation energy ( $E_D$ ) of NBO-free glass (purely silica glass) is within the range of 20–120 kJ/mol, while for NBO-bearing glass it ranges between 25 and 50 kJ/mol. However, the composition of glass mixture might vary the value of  $E_D$  in NBO-bearing glass. The Region II was observed at temperature range of 500 °C to 700 °C; and showed an anomalous decreasing rate constant with increasing temperature. Again, this observation was highly related to the formation of viscous glass structure which started to form at temperatures above 500 °C. This phenomenon is an indication that support the diffusion-controlled mechanism during the PbO–SiO<sub>2</sub> pellets reduction.

#### E. Reaction Mechanism

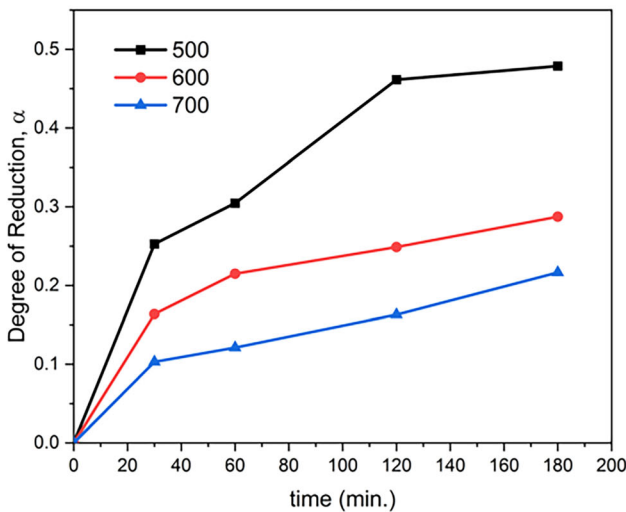
Considering the results presented in the previous sections, two generic mechanisms of the reduction of PbO–SiO<sub>2</sub> pellets were proposed. The mechanisms were classified based on the softening point of the glass (below and above) as schematically presented in Figure 16. The first mechanism is for the reduction at temperatures below the softening point. This corresponds to the Region I in Figure 15. In this mechanism, the process appeared to mainly involves hydrogen reduction at microscopic scale which eventually resulted in the formation and aggregation of Pb that is embedded within the glass. The reduction presumably started by hydrogen diffusion through amorphous glass structure and the reaction would start at preferred sites with a metastable equilibrium in the silicate network, that is where the ionic Pb located. The Pb–O bonds are much weaker compared to Si–O bonds. The high concentration of PbO in the lead silicate would provide many Pb ion as network modifier, hence also provided many sites for the hydrogen reduction and Pb nucleation to occur. It is noteworthy that reduction in this Region I occurred before the glass turn viscous, thus, the hydrogen was able to reach into the interior of the sample for continued reduction. The H<sub>2</sub>O gas product also appeared to able to diffuse out from the sample, and overall there was no shape change on the sample during the reduction.

**Table IV. Calculated Values of NBO/T, DoP, and Q<sup>3</sup> Position from the Measured Spectra**

| Sample           |                    | Q <sup>3</sup> Position | NBO/T  | DoP (Q <sup>3</sup> + Q <sup>4</sup> )/(Q <sup>0</sup> + Q <sup>1</sup> ) |
|------------------|--------------------|-------------------------|--------|---|
| Temperature (°C) | Reduction Time (h) |                         |        |   |
| 300              | 0                  | 1060.82                 | 212.6  | 0.79  |
|                  | 0.5                | 1057.98                 | 258.06 | 0.24  |
|                  | 1                  | 1056.95                 | 237.88 | 0.29  |
|                  | 3                  | 1037.01                 | 228.57 | 0.52  |
| 400              | 0                  | 1060.82                 | 212.6  | 0.79  |
|                  | 0.5                | 1050.43                 | 245.00 | 0.31  |
|                  | 1                  | 1045.83                 | 230.80 | 0.34  |
|                  | 3                  | 1043.19                 | 232.33 | 0.30  |



(a)



(b)

Fig. 13—Degree of reduction as a function of time of the PbO–SiO<sub>2</sub> pellet samples reduced in 15 pct H<sub>2</sub>–N<sub>2</sub> atmosphere at temperatures (a) 300 °C to 500 °C, and at (b) 500 °C to 800 °C.

The second mechanism for reduction at temperatures above softening point, which is marked Region II in Figure 15, involves hydrogen reduction at microscopic scale accompanied by glass softening at macroscale. The softening process (formation of viscous materials) has different pace between samples reduced at 600 °C and 700 °C. As evidenced from samples' cross-section observation and XRD analyses, the Pb nucleation at microscopic scale occurred at the early minutes. In the case of reduction of samples at 600 °C, the reduction managed to occur further into the interior of the sample before shrinkage and extensive softening occurred. In the case of the reduction at 700 °C, it appeared that the softening occurred earlier and provided barrier for diffusion of hydrogen (and H<sub>2</sub>O gas product), hence the reduction could only have occurred effectively on the surface. The viscous material formed also promoted the bubble formation (trapped gas bubbles within the sample). This observation was also supported by the kinetics result where the reduction degree of samples reduced at 600 °C was higher than samples reduced at 700 °C. The cross section and SEM evidences strongly supported that the blackish region on the surface of the sample at 700 °C were reduced while the centre is unreduced. In this second mechanism, the viscous state of the matter also meant that the overall shape of the pellets changed during the reduction. When the majority part of sample state become more viscous, the pellet tends to form a round shape due to its high surface tension.

From the reaction mechanism analysis above, it suggests an important information regarding a possible practice for industrial process context. In industry, to achieve quite extensive reduction from PbO–SiO<sub>2</sub> materials, a viscous condition should be avoided, *i.e.*, the reduction should be carried out either below the softening point or at the conditions of fully liquid (well above the liquidus). Viscous state of the material was evidently hinder further hydrogen reduction into high degree reduction.

**Table V. Calculated  $k$  (Rate Constant) and  $R^2$  (Regression Linier Coefficient) from Fitting of Various Solid–Gas Kinetic Models for the Reduction of PbO–SiO<sub>2</sub> Samples at 300 °C to 700 °C**

| Kinetics Model                             | 300 °C   |             | 400 °C  |             | 500 °C |             | 600 °C  |             | 700 °C  |             |
|--|----------|-------------|---------|-------------|--------|-------------|---------|-------------|---------|-------------|
|  | $k$      | $R^2$       | $k$     | $R^2$       | $k$    | $R^2$       | $k$     | $R^2$       | $k$     | $R^2$       |
| A2 ( $-\ln(1-\alpha)^{1/2}$ )              | 0.0003   | 0.84        | 0.001   | 0.93        | 0.0023 | 0.94        | 0.0012  | 0.9         | 0.0008  | 0.95        |
| A3 ( $-\ln(1-\alpha)^{1/3}$ )              | 0.0002   | 0.84        | 0.0007  | 0.93        | 0.0019 | 0.97        | 0.0008  | 0.9         | 0.0005  | 0.95        |
| A4 ( $-\ln(1-\alpha)^{1/4}$ )              | 0.0001   | 0.84        | 0.0005  | 0.93        | 0.0011 | 0.94        | 0.0006  | 0.9         | 0.0004  | 0.95        |
| R1 ( $\alpha$ )                            | 0.0005   | 0.83        | 0.0017  | 0.92        | 0.0034 | 0.92        | 0.002   | 0.89        | 0.0014  | 0.94        |
| R2 ( $1-(1-\alpha)^{1/2}$ )                | 0.0003   | 0.84        | 0.0009  | 0.93        | 0.0019 | 0.93        | 0.0011  | 0.89        | 0.0007  | 0.94        |
| R3 ( $1-(1-\alpha)^{1/3}$ )                | 0.0002   | 0.84        | 0.0006  | 0.93        | 0.0014 | 0.93        | 0.0007  | 0.90        | 0.0005  | 0.94        |
| D1 ( $\alpha^2$ )                          | 0.00004  | 0.91        | 0.0004  | 0.97        | 0.0015 | 0.97        | 0.0005  | 0.97        | 0.0003  | 0.99        |
| D2 ( $\alpha + (1-\alpha) \ln(1-\alpha)$ ) | 0.00002  | 0.91        | 0.0002  | 0.97        | 0.0009 | 0.98        | 0.0003  | 0.97        | 0.0001  | 0.99        |
| D3 ( $(1-(1-\alpha)^{1/3})^2$ )            | 0.000004 | <b>0.91</b> | 0.00005 | <b>0.97</b> | 0.0003 | <b>0.98</b> | 0.00007 | <b>0.98</b> | 0.00003 | <b>0.99</b> |
| D4 ( $1-2\alpha/3-(1-\alpha)^{2/3}$ )      | 0.000004 | <b>0.91</b> | 0.00005 | <b>0.97</b> | 0.0002 | <b>0.98</b> | 0.00006 | <b>0.97</b> | 0.00003 | <b>0.99</b> |

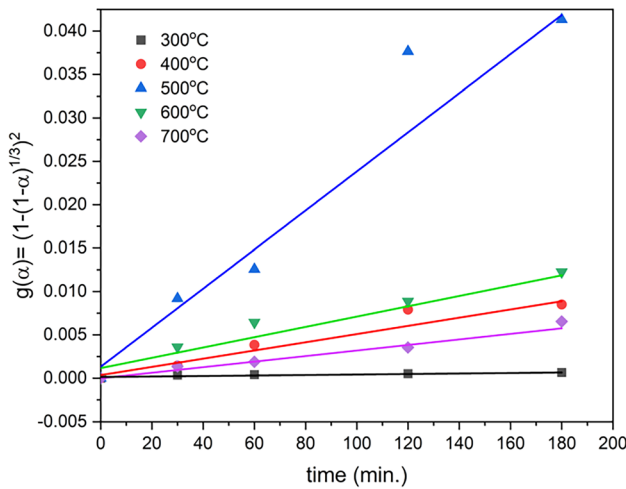


Fig. 14—A plot of kinetics data of PbO–SiO<sub>2</sub> pellets reduction by hydrogen at 300 °C to 700 °C using the Jander model.

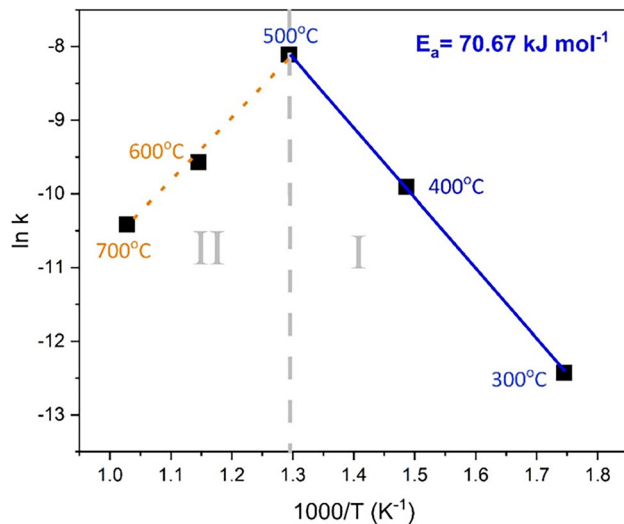


Fig. 15—Arrhenius plot on using Jander model showing two kinetics regions, *i.e.*, Region I, where the rate is increasing with temperature and Region II where the rate is decreasing with temperature.

#### IV. CONCLUSIONS

A study of reduction of 70 wt pct PbO–30 wt pct SiO<sub>2</sub> by hydrogen at temperatures from 300 °C to 700 °C has been carried out. Sequences of macro and microstructure studies, supported by phase analysis from XRD, EDS, and Raman spectroscopy were conducted resulting on findings as the followings:

- Macrograph observation at temperature range of 300 °C to 500 °C the macrograph results showed a gradual colour change from white unreduced sample into brownish and blackish, where it is confirmed by SEM, EDS and XRD analysis that this happened due to the formation of Pb that was embedded within the glass. While, reduction at 600 °C and 700 °C immediately change the sample into blackish at early of reduction which followed by the formation viscous structure.
- The silicate structure analysis using Raman spectroscopy revealed that there was a shift in the  $Q^3$  position as the reduction reaction was progressing at 300 °C and 400 °C. The calculated degree of polymerisation (in this case  $(Q^3 + Q^4)/(Q^0 + Q^1)$ ) and the NBO/T did not provide a clear trend with increasing reduction time.
- Overall reduction of lead silicate appeared to follow a diffusion-controlled process at temperature region of 300 °C to 500 °C. The apparent energy activation was calculated to be 70.7 kJ/mol.
- At higher temperatures of 600 °C and 700 °C, pellets started to sinter, and then viscous material was formed due to the softening phenomenon. This provided a barrier for further hydrogen reduction, hence significantly affected the kinetics of lead silicate reduction. Between 500°C to 700°C, the reduction rate was observed to decrease with increasing temperature due to the phenomenon.

The findings from the current study give an industrial implication that regardless the kinetics rate, to obtain a complete reduction process either a solid state or complete molten phase are preferred over a viscous state. Therefore, a condition in within viscous range needs to be carefully identified and considered.



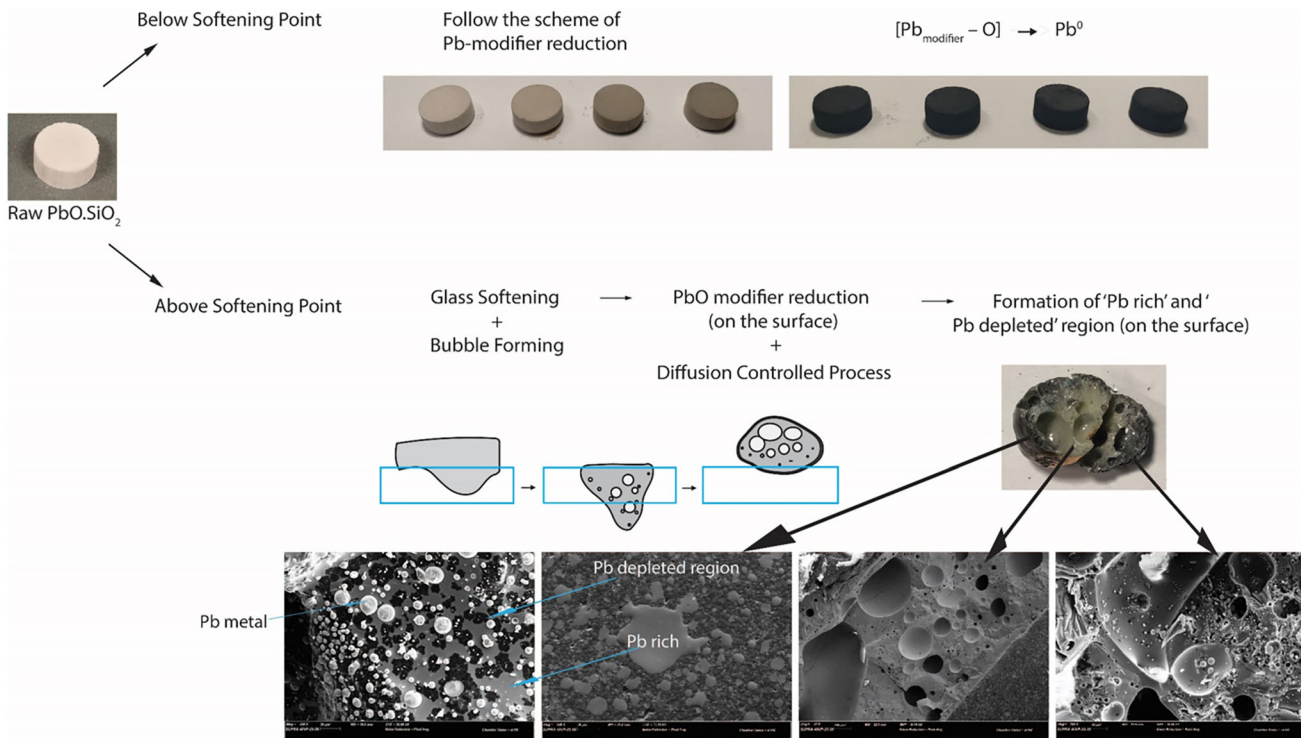


Fig. 16—Illustration of proposed mechanisms of hydrogen reduction of PbO–SiO<sub>2</sub> pellets.

## ACKNOWLEDGMENTS

The authors are grateful to Umicore Belgium and Swinburne University of Technology Australia for providing funding for the current study through joint SUPRA (Swinburne University Postgraduate Research Award) scholarship for PhD study of Asywendi Rukini.

## FUNDING

Open Access funding enabled and organized by CAUL and its Member Institutions.

## CONFLICT OF INTEREST

The authors declare that they have no conflict of interest.

## OPEN ACCESS

This article is licensed under a Creative Commons Attribution 4.0 International License, which permits use, sharing, adaptation, distribution and reproduction in any medium or format, as long as you give appropriate credit to the original author(s) and the source, provide a link to the Creative Commons licence, and indicate if changes were made. The images or other third party material in this article are included in the article's Creative Commons licence, unless indicated otherwise in a credit line to the material. If material is not included in the article's Creative Commons licence

and your intended use is not permitted by statutory regulation or exceeds the permitted use, you will need to obtain permission directly from the copyright holder. To view a copy of this licence, visit <http://creativecommons.org/licenses/by/4.0/>.

## REFERENCES

1. N.N. Kinaev, E. Jak, and P. Hayes: *Scand. J. Metall.*, 2005, vol. 34, pp. 150–57.
2. S. Jahanshahi and S. Wright: *Metall. Mater. Trans. B*, 2017, vol. 48B, pp. 2057–66.
3. C. Wang, K. Li, H. Yang, and C. Li: *ISIJ Int.*, 2017, vol. 57(6), pp. 996–1003.
4. R. Vanparys, G. Brooks, M.A. Rhamdhani, and T. Crivits: *Reduction of lead-rich slags with coke in the lead blast furnace, PbZn 2020: The 9th International Symposium on Lead and Zinc Processing TMS* (2020).
5. ILZSG Report: The World Lead Factbook 2019, International Lead and Zinc Study Group [https://www.ilzsg.org/wp-content/uploads/SitePDFs/1\\_ILZSG%20Lead%20Factbook.pdf](https://www.ilzsg.org/wp-content/uploads/SitePDFs/1_ILZSG%20Lead%20Factbook.pdf), accessed 24 July 2023.
6. K.B. Blodgett: *J. Am. Ceram. Soc.*, 1951, vol. 34, pp. 14–27.
7. Y. Huang, Y. Zhang, H. Liu, and Z. Gu: XPS study on microporous surface composition of microchannel plates. in *Proc. SPIE 8194, International Symposium on Photoelectronic Detection and Imaging 2011: Advances in Imaging Detectors and Applications, 81941Q* (18 August 2011); <https://doi.org/10.1117/12.900283>.
8. Y. Zhang, Y. Sun, J. Wang, K. Huang, Y. Wang, J. Liu, B. Zhang, W. Hou, and X. Lu: *IOP Conf. Ser.*, 2018, vol. 423, p. 012167.
9. P.W. Wang and L. Zhang: *J. Non-Cryst. Solids*, 1996, vol. 194, pp. 129–34.
10. O.M. Kannunikova, F.Z. Gilmutdinov, and A.A. Shakov: *Int. J. Hydrog. Energy*, 2002, vol. 27, pp. 783–91.
11. L. Robinet, A. Bouquillon, and J. Hartwig: *J. Raman Spectrosc.*, 2008, vol. 39, pp. 618–26.

12. P. Colomban, A. Tournie, and L. Bellot-Gurnlet: *J. Raman Spectrosc.*, 2006, vol. 37, pp. 841–52.
13. C.A. Worrell and T. Henshall: *J. Non-Cryst. Solids*, 1978, vol. 29, pp. 283–99.
14. A. Khanna, A. Kaur, M. Fabian, Hirdesh, and A. Kaur: *Indian J. Phys.*, 2021, vol. 95(10), pp. 2187–99.
15. T. Furukawa, S.A. Brawer, and W.B. White: *J. Mater. Sci.*, 1978, vol. 13, pp. 268–82.
16. I.B. Kacem, L. Gautron, and D.R. Coillot: *Chem. Geol.*, 2017, vol. 461, pp. 104–14.
17. U.B. Pal, T.D. Roy, and G. Simkovich: *Metall. Trans. B*, 1983, vol. 14B, pp. 693–701.
18. A. Rukini, M.A. Rhamdhani, G.A. Brooks, and A. Van den Bulck: *Metall. Mater. Trans. B*, 2023, <https://doi.org/10.1007/s11663-023-02745-0>.
19. J.O. Bockris and G.W. Mellor: *J. Phys. Chem.*, 1956, vol. 60, pp. 1321–28.
20. H.W. Nesbitt and M.E. Fleet: *Geochim. Cosmochim. Acta*, 1981, vol. 45, pp. 235–44.
21. J. Szekely, C.I. Lin, and H.Y. Sohn: *Chem. Eng. Sci.*, 1973, vol. 28, pp. 1975–89.
22. A. Khawam and D.R. Flanagan: *J. Phys. Chem. B*, 2006, vol. 100(35), pp. 17315–28.
23. H.S. Ray and S. Ray: *Chapter 11: Analysis of Kinetics Data for Practical Application, Kinetics of Metallurgical Processes*, 2018, pp. 315–39.
24. A. Shrivastava: *Introduction to Plastics Engineering*, Plastics Design Library William Andrew, 2018, pp. 1–16.
25. R.F. Tournier and M.I. Ojovan: *Materials*, 2021, vol. 9(4), p. 2287.
26. A.G.S. Filho, I. Guedes, P.T.C. Freire, J.M. Filho, M.C.C. Custodio, R.M. Lebullenger, and A.C. Hernandes: *J. Raman Spectrosc.*, 1999, vol. 30, pp. 525–29.
27. B.O. Mysen: *Annu. Rev. Earth Planet. Sci.*, 1983, vol. 11, pp. 75–79.
28. J.H. Park: *Met. Mater. Int.*, 2013, vol. 19, pp. 577–84.
29. M.M. Hasan, PhD Thesis, Swinburne University of Technology, 2022.
30. M.M. Hasan, M.A. Rhamdhani, M.A.H. Shuva, and G.A. Brooks: *Metals*, 2020, vol. 10(1), p. 78.
31. J.H. Park: *J. Non-Cryst. Solids*, 2012, vol. 358(23), pp. 3096–3102.
32. Z. Zhang, B. Xie, W. Zhou, J. Diao, and H.-Y. Li: *ISIJ Int.*, 2016, vol. 56(5), pp. 828–34.
33. M. Zhao, J. Cao, Z. Wang, and G. Li: *J. Non-Cryst. Solids*, 2019, vol. 513, pp. 144–51.
34. E. Segal: *Rev. Roum. Chim.*, 2012, vol. 57(4–5), pp. 491–93.
35. T. Walter, R. Muller, J. Deubener, U. Marzok, and S. Reinsch: *Front. Mater.*, 2020, vol. 6, pp. 1–7.

**Publisher's Note** Springer Nature remains neutral with regard to jurisdictional claims in published maps and institutional affiliations.